Tino Stanković[1]
Engineering Design and Computing Laboratory,
Department of Mechanical and Process Engineering,
ETH Zürich,
Tannenstr. 3, 8092 Zürich, Switzerland
e-mail: tinos@ethz.ch

Jochen Mueller
Mem. ASME
Engineering Design and Computing Laboratory,
Department of Mechanical and Process Engineering,
ETH Zürich,
Tannenstr. 3, 8092 Zürich, Switzerland
e-mail: jm@ethz.ch

Paul Egan
Mem. ASME
Engineering Design and Computing Laboratory,
Department of Mechanical and Process Engineering,
ETH Zürich,
Tannenstr. 3, 8092 Zürich, Switzerland
e-mail: pegan@ethz.ch

Kristina Shea
Mem. ASME
Engineering Design and Computing Laboratory,
Department of Mechanical and Process Engineering,
ETH Zürich,
Tannenstr. 3, 8092 Zürich, Switzerland
e-mail: kshea@ethz.ch

A Generalized Optimality Criteria Method for Optimization of Additively Manufactured Multimaterial Lattice Structures

Recent progress in additive manufacturing (AM) allows for printing customized products with multiple materials and complex geometries that could form the basis of multimaterial designs with high performance and novel functions. Effectively designing such complex products for optimal performance within the confines of AM constraints is challenging due to the need to consider fabrication constraints while searching for optimal designs with a large number of variables, which stem from new AM capabilities. In this study, fabrication constraints are addressed through empirically characterizing multiple printed materials' Young's modulus and density using a multimaterial inkjet-based 3D-printer. Data curves are modeled for the empirical data describing two base printing materials and 12 mixtures of them as inputs for a computational optimization process. An optimality criteria (OC) method is developed to search for solutions of multimaterial lattices with fixed topology and truss cross section sizes. Two representative optimization studies are presented and demonstrate higher performance with multimaterial approaches in comparison to using a single material. These include the optimization of a cubic lattice structure that must adhere to a fixed displacement constraint and a compliant beam lattice structure that must meet multiple fixed displacement constraints. Results demonstrate the feasibility of the approach as a general synthesis and optimization method for multimaterial, lightweight lattice structures that are large-scale and manufacturable on a commercial AM printer directly from the design optimization results.
[DOI: 10.1115/1.4030995]

1 Introduction

Current advances in AM enable the multimaterial fabrication of three-dimensional (3D) objects that are difficult or impossible to create with conventional manufacturing technologies [1–3]. When AM technologies are utilized in combination with computational optimization methods, it is possible to control the distribution of materials within objects with a high degree of precision [4]. Such precision in creating products has the potential to dramatically improve structural performance and even enable new functionalities through careful placement of multiple materials throughout a structure [5]. However, such precision in material distribution leads to an increase in complexity when designing products that are already challenging to design when only single materials are considered, such as lattice structures [6]. Lattice structure design is typically approached using computational optimization methods due to the need for considering many variables in configuring high-performance structures [7,8]. A further challenge in effective AM design is the need for solutions found by computational optimization to remain printable according to design for additive manufacturing (DfAM) constraints, such as the limitations in tolerances, printable dimensions, and quality issues incurred by the fabrication process [9–12]. In this paper, we address these challenges in creating AM optimized designs by developing an optimization approach that utilizes empirical measurements of AM materials to configure multimaterial lattices.

The design of high-performance, multimaterial lattices for complex shapes has particular applications in developing customized sport helmets with impact resistance [13,14]. Lattice structures are growing in interest due to their improved strength-to-weight ratio compared with stochastic foams alone. When lattices are utilized in combination with stochastic foams, the combination sometimes shows superior performance for both strength and energy absorption, which are both necessary for effective helmet performance [15]. Additionally, AM processes enable the construction of lattices tailored for specific products that were not achievable with past manufacturing methods. A proposed DfAM methodology for the complete design and fabrication of a customized product [16], such as a sport helmet with multimaterial lattices, includes phases for (1) characterizing AM materials, processes, and structure, (2) developing quantitative and simulation models to accurately predict behavior, (3) optimizing designs with computational methods, and (4) fabricating and testing a resulting multimaterial product (Fig. 1). Once fabrication is completed, findings are informative for future product design cycles such as further characterization of AM materials, processes, and structures or refinement of quantitative and simulation models.

Due to the large scope of the DfAM methodology (Fig. 1), this paper primarily focuses on the computational design and optimization phase with a secondary focus on the AM characterization, i.e., how the optimization method utilizes information of multiple AM characterized materials and processes to configure a printable product. Since the total volume of the helmet is constrained based on user requirements, design decisions concerning material changes in the lattice are beneficial because they can alter the product's performance capabilities without altering its

[1]Corresponding author.

Early iterations of this work were accepted to the 2015 ASME Computers and Information in Engineering Conference (Stanković et al. 2015).

Contributed by the Design for Manufacturing Committee of ASME for publication in the Journal of Mechanical Design. Manuscript received February 15, 2015; final manuscript received June 15, 2015; published online October 12, 2015. Assoc. Editor: Timothy W. Simpson.

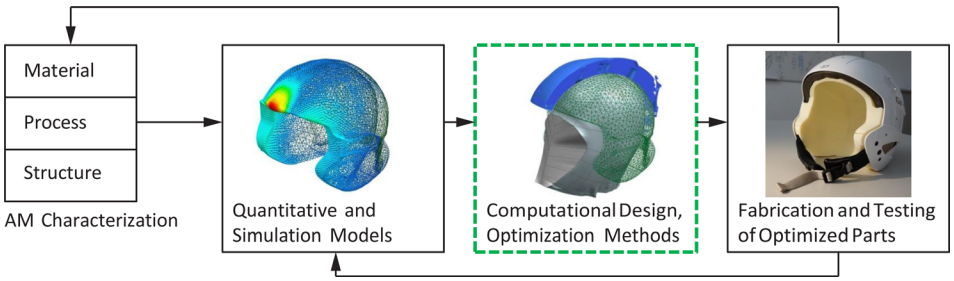

Fig. 1 DfAM product design methodology

dimensions. The use of AM for producing the helmet is particularly beneficial, since it enables customized helmet shapes on a per-consumer basis such that the helmet conforms to a particular customer's head shape and has performance requirements that are tailored to particular applications [14,17,18]. Due to these considerations for the helmet, multimaterial AM could greatly facilitate its design in comparison with conventional manufacturing approaches. These are demonstrated through two optimization problems in the paper: a cubic lattice that is optimized for a given displacement to maximize its performance in a fixed volume and a beam lattice that is optimized for maximum performance for multiple displacement constraints.

There is a need to investigate effective optimization algorithms for multimaterial AM, since such optimization problems have so far only been considered for a limited set of problems and applications [5,7], typically more on the microstructure level. New methods are particularly needed because established evolutionary-based and other metaheuristic methods have difficulty in optimizing large, complex structures, because they do not scale well as the resolution and number of structural members in an application increases. In the helmet example, however, the full structural design could require optimization of hundreds to hundreds of thousands of members. Other algorithms that are well-suited for structural optimization, such as the discrete OC method [8], are appropriate for large discrete- and lattice-based structures, but have no current formulation for solving multimaterial problems. Most often, the problem formulation for OC methods is a purely mass-based optimization and considers dominant displacement constraints only [8]. However, more constraint rich applications exist [19,20] in addition to the possibility for extending the method to solve multimaterial lattices.

In this paper, we focus on developing a generalized OC method [21] for the optimization of discrete, multimaterial, mesoscale lattice structures for maximum performance in a constrained volume. Through considering the formulation of the optimization algorithm within the context of a DfAM methodology (Fig. 1), the optimization approach is developed to integrate information about AM characteristics of materials and processes that ensures the optimized design can be directly fabricated with AM. Experimental testing is conducted to determine the properties of two AM materials that the optimization algorithm may combine in different mixtures to design lattices with varied properties. The optimization algorithm is then developed through using OC derived for lattice structures to configure two representative examples related to the helmet lattice functional requirements. The paper seeks to present a generalizable synthesis and optimization method for the design and AM fabrication of multimaterial structures that can form the basis for a variety of customized products.

2 Background

In this section, background work is presented detailing general lattice optimization approaches and recent endeavors in designing products using multimaterial AM techniques. OC methods are then reviewed to assess their feasibility for discrete lattice optimization applications.

2.1 Lattice Optimization. Although there are currently no preferred optimization approaches for multimaterial lattices, there are a large number of existing approaches for single material lattice structure optimization, such as the size matching and scaling method [22]. The size matching and scaling method has been implemented to design and optimize mesoscale, cellular lightweight structures. The method couples a library of predefined unit cells with solid body finite element analysis that is applied over a design domain to provide a design response to guide unit cell selection, scaling, and placement. The size matching and scaling method demonstrated better performance than the particle swarm based lattice optimization [23] and the least squares fitting method [23] when applied for a predefined topology or ground structure optimization.

A different approach from Ning and Pellegrino [24] aims to design and optimize lattices through consideration of the microstructure of lightweight sandwich beam designs within a size distribution field using multiple optimization steps. Using Delaunay triangulation, the 2D topology search is reduced to a limited number of continuous control variables. The first step in the optimization approach is to utilize a genetic algorithm (GA) to optimize the topology, and then lattice truss cross section sizes are optimized using the best topology found.

In generative design and optimization of macroscale lattice structures, a different approach to the previous one is explored in previous work by one of the authors for the generative synthesis of transmission towers [25]. The search for the optimal topology, member sizes, and performance is achieved through a combination of graph-grammars and a shape annealing method to create spatially novel designs. These examples demonstrate that past approaches developed solutions for effective topology, shape, and cross section optimization, while new methods could contribute to optimization with respect to material choice, specifically for configuring discrete lattices for AM, as considered in this paper.

2.2 Multimaterial AM. Unlike conventional manufacturing, AM is a fabrication process that joins materials layer by layer to build a part based on the computer-aided design model data. Effective design for AM requires the consideration of processes including the time-required for the product fabrication, the materials used, and the mechanical properties [26–28]. Multimaterial applications are particularly relevant to AM because they enable a more precise optimization of the mechanical properties of parts and provide additional functionality [2], such as fabricated materials with desired deformation behavior [29,30]. There is also the possibility of including gradients of different materials throughout a part using multimaterial AM. Such possibilities have been investigated with optimization methods for the manufacturing of heterogeneous 3D objects considering mechanics-fabrication tradeoffs for a single I-beam using a self-adaptive evolutionary strategy that is well-suited for multimodal problems [31]. Multiple-material topology optimization has also been investigated in the context of AM for 2D material structures considering deflection in a structure using a compliant mechanism-based optimization process [5]. These studies demonstrate the potential benefits of multimaterial

AM applications and the need for further developing optimization methods in solving the resulting complex and large-scale design problems.

2.3 OC Methods. In addition to already established lattice and multimaterial optimization approaches, there is the opportunity to tailor optimization approaches from other applications in discrete structural optimization for lattice design, with OC being a potentially highly effective approach. In the late 1960s, OC methods were developed to tackle the large-scale structural optimization of discrete member structures for the aerospace industry [8,19,32,33]. Early applications of OC considered static load cases with displacement constraints only, but the method was soon extended to consider stress and buckling constraints in addition to stability, and for impact and frequency responses [34,35]. To balance computational efficiency with solution quality for application to large-scale problems, a heuristic-based fully constrained design method was developed [36]. This method is not gradient-based and overcomes the requirement that the OC algorithm needs for customization of each unique problem formulation. However, the method is only applied to displacement constraints. Another successful application is the optimization of tall steel buildings extending the OC method to include commercial standard sections in the optimization [37].

The primary motivation for the development of the OC approach was to address the inability of conventional mathematical programming methods to handle optimization problems that exceed 200–300 design variables for a generic case of a statically indeterminate structure with a nonlinear constraint set [8,19]. This bears resemblance to the case considered in this paper of multimaterial, lattice structures fabricated with AM. Before the OC method was developed as an approach, numerous alternative search strategies and problem simplifications were applied to handle these issues, but were not highly effective. For example, variable linking and problem order decrease approaches are hard to implement due to the difficulty in assessing the implications of these actions to the overall optimized solution. The direct consequence of using OC is a reduction of cost in required iteration steps to obtain a significant improvement in the objective function, with respect to the size of the variable vector [19]. The OC approach additionally requires the calculation of a pseudo-energy function that is obtained when a finite element method is applied to calculate a design response [38], which further motivates it as potentially effective for multimaterial lattice optimization applications.

3 Motivation for Using OC

Findings from the literature review suggest that the development of an efficient lattice structure optimizer that handles a large set of different design variables and constraints requires further research. Stochastic methods, e.g., simulated annealing and GAs, are generally robust, i.e., different problem formulations and constraints can be readily included, but experience problems, e.g., computational time, when the number of variables becomes too large. Least squares fitting methods, such as the design of experiments based responsive surface methods, are another possible approach that alleviates computational costs by using a surrogate approach, but are also limited in finding high quality solutions for large-scale structures of 10,000 or more members. With respect to the complexity of discrete lattice structures that are producible using AM, the application of OC for parametric optimization offers the benefit of decoupling the variable vector size and required iteration steps, which is suggestive of its potential for effectively optimizing large-scale lattice structures with multiple materials.

To assess the OC method's feasibility in comparison to other optimization methods for complex lattice structures, it is benchmarked against the canonical GA from our own GA framework and interior point optimization from the MATLAB optimization toolbox. These methods are compared using a test-case lattice with 74 members that occupies a space of $50 \times 50 \times 50$ mm^3 and is optimized for minimum mass when taking cross-sectional area A_i as the design variable. A recursive resizing formula that is a special simplified case of OC is applied and referred to as the fully stressed design (FSD) approach. FSD is easily extendible for the lattice application, fast in convergence, but is an oversimplification of the OC method because it limits the possibilities to express multiple constraints, load conditions, and the application of different materials. Therefore, FSD is a viable approach for benchmarking the feasibility of OC in comparison to other methods, but is not suitable for complex multimaterial lattice structures subject to different constraints and loading conditions. The recursive sizing formula for the cross-sectional area A_i of a steel lattice structure in the test-case is [7]

$$A_i^{\nu+1} = \left(\frac{U_i A_i^{\nu}}{\varepsilon_i^2 \rho_i l_i}\right)^{1/2} \tag{1}$$

where ν denotes the iteration step U_i, the current strain energy stored in the ith element $\rho_i = 7860$ kg/m^3 is the density, l_i is the length of the ith element, and ε_i is the allowed strain per element calculated for $E = 206$ GPa and allowed stress $|\sigma| \leq 50$ N/mm^2. Buckling and displacement constraints are not taken into account. The load of $F = 1000$ N is distributed among all nodes of the lattice top face in the direction of the negative z-axis, while the bottom face nodes are fully constrained. The variable range is defined as $0.01\,\text{mm}^2 \leq A_i \leq 10\,\text{mm}^2$. The results for the starting point of $A_i = A = 10$ mm^2 are shown in Fig. 2 and indicate the benefits of the OC method, as demonstrated by the FSD approach having found the lightest structure (11.81 g) with less run-time (less than 10 s) and iterations (20) in comparison to both other methods.

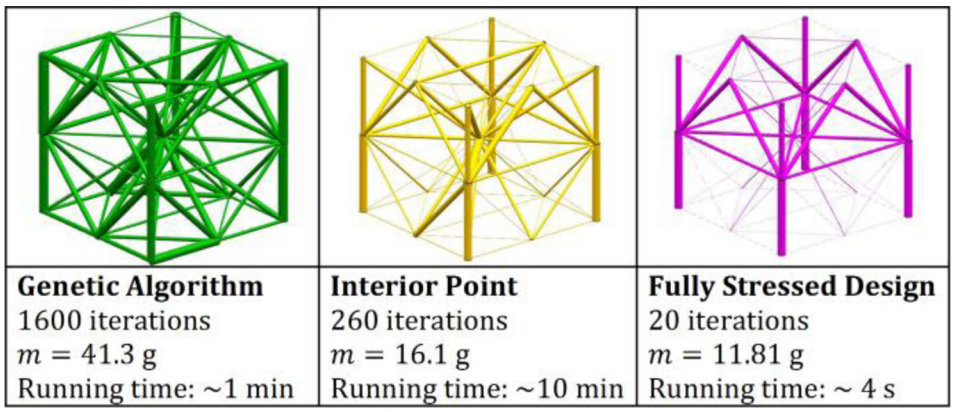

Fig. 2 Results of benchmarking algorithms for a steel lattice test-case

Although there are many benefits in using OC approaches with respect to computational time-required to optimize large-scale structures, its context oriented basis lacks generality that hinders its efficient use [21]. The OC are most commonly expressed to meet the specific features of a design for particular applications. In an effort to mitigate this limitation, a generalized OC method was developed [21] by extending the OC application to general multidisciplinary optimization problems by offering a methodological approach in both recursive algorithm derivation as well as in the application of compound scaling algorithm. The search strategy is then based on a recursive sweep through the search space while applying scaling procedures to estimate the location of constraints boundaries [21]. This generalized formulation of the OC is considered in this paper and extended for multimaterial lattice structure optimization problems.

4 Characterization of AM Materials

To optimize lattice structures according to AM constraints, empirical studies are performed to characterize AM materials that are then input into the optimization model. These steps include testing and measurement of material properties and then fitting curves to describe the data that are then used in the optimization method.

4.1 Materials Testing Methods. To facilitate multimaterial lattice design, Young's modulus (E) and density (ρ) are measured for different AM materials. The measurements are obtained using a Stratasys Objet500 Connex3 due to the printer's capabilities for printing up to three different model materials at the same time, thus enabling the fabrication of multimaterial lattices. The printer's support material is a wet mixture of SUP705 support and a generic model material. The liquid material is jetted onto the surface and immediately cured with UV light positioned on the print head. A pinch roll ensures a smooth and clean surface when jetting the next layers.

In the printer's digital material mode, model materials are mixed to create combinations of properties such as a hard and a soft material with mixed properties in between. The potential to mix materials is highly beneficial for lattice applications, because with just two base material choices there is a broad range of intermediate mixes of materials with unique properties. In order to have a broad range of material performance properties, materials of low and high strength are tested that are referred to as TangoBlackPlus and VeroWhitePlus by the manufacturer and chosen based on the mechanical properties provided by the manufacturer. The manufacturer reported performance of VeroWhitePlus is $E = 2000 - 3000$ MPa, UTS $= 50 - 65$ MPa, and $\rho = 1.17 - 1.18$ g/cm^3, while the manufacturer only reported TangoBlackPlus values of UTS $= 0.8 - 1.5$ MPa and $\rho = 1.12 - 1.13$ g/cm^3 [39]. Testing is conducted to verify these performance values, in addition to measuring values such as the mixed material properties that are not provided by the manufacturer.

Testing samples are printed for each of the 14 possible material gradings available for printing based on constraints from the manufacturer and are inclusive of the two base materials. Testing commenced on an Instron ElectroPuls E3000 tensile testing machine that enables the testing of the mechanical properties according to the ASTM D638-10 standard. Additionally, materials are weighed with a Metler Toledo XS205 DualRange scale. For each material grading, one measurement is collected due to negligible variations in measurements of parts produced on the same machine in controlled conditions [40]. Based on data from the manufacturer concerning minimum printable dimensions of a structure [41], strut diameters of 1 mm are used to generate samples.

4.2 Materials Testing Results. For all 14 printed materials, the density of the material is calculated as an independent variable and plotted against the measured Young's modulus (Fig. 3). The Young's modulus, as a function of the density, can then be directly calculated from a fitted curve.

The plot in Fig. 3 demonstrates that the densities of the 14 materials have an uneven distribution over the range of 1.09 g/cm^3 to 1.175 g/cm^3, with most materials being close to the extremes. The plot also includes the manufacturer's reported data for comparison, which are only available for a limited set of density values. The experimental measurements for the Young's modulus obtained are higher than those provided by the manufacturer [39] (Fig. 3). Generally, materials are bimodally distributed around Young's modulus values of about 50 MPa and 2800 MPa. Due to the limited number of material mixtures available in the printer as a result of manufacturer software limitations, there is a lack of testable material mixtures that may fall in the intermediate range. The data suggest that material properties are generally below 500 MPa for densities below 1.14 g/cm^3 with a sharp increase to about 3000 MPa for materials with density above 1.14 g/cm^3. A curve is fit to the data, since the optimization algorithm requires continuous functions to calculate material properties. For the optimization model, a sigmoidal curve of shape

$$E(\rho) = A_1 + \frac{A_2 - A_1}{1 + 10^{(\log(x_0) - \rho)\cdot p}} \tag{2}$$

is fit to the values (black solid line, adjusted R-square of 0.99794) where A_1 and A_2 represent the lower and upper asymptotes, p is the hill slope, and x_0 the center point. Solving the equation for ρ, which is required for the model input, yields the following equation:

$$\rho(E) = \log x_0 - \frac{\log\left(\frac{A_2 - A_1}{E - A_1} - 1\right)}{p} \tag{3}$$

The material characterization demonstrates the properties and relations that are used by the computational optimization algorithm to only search for designs with properties that are possible to fabricate with the AM technology considered here. While the current commercial machine used in this investigation only allows printing of the 14 discrete materials tested through a software block, in principle the technology can print continuous mixtures of the materials, as modeled by the curve.

5 Generalized OC Using Multimaterials

With respect to the complexity of discrete lattice structures that are produced using AM technologies, the application of OC for

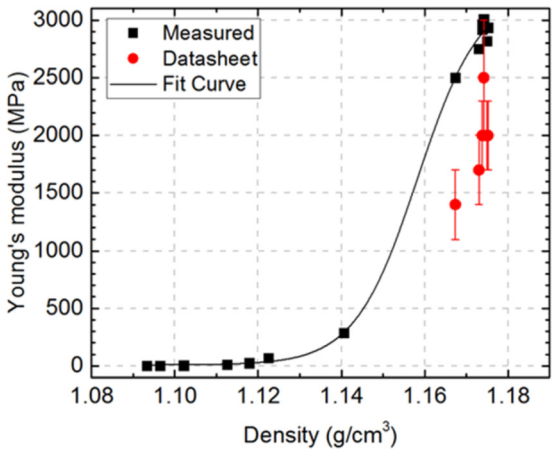

Fig. 3 Empirical AM data for Young's modulus as a function of density. Shown are the experimentally obtained values (rectangle), the values taken from the materials' datasheets (circle), and the fitted curve.

parametric optimization offers the key advantage of decoupling the variable vector size and required iteration steps that are required for effectively optimizing large-scale lattice structures with multiple materials. In this context, the OC are defined by the conditions that are satisfied at the optimum point only [8,19,21], providing a system of n equations with m active constraints

$$\sum_{j=1}^{m} e_{ij}\lambda_j = 1 \tag{4}$$

where λ_j is Lagrangian multiplier corresponding to the jth constraint, and e_{ij} is the ratio of sensitivity derivates

$$e_{ij} = \frac{N_{ij}}{\nabla F_i} = \frac{\dfrac{\partial z_j}{\partial x_i}}{\dfrac{\partial F}{\partial x_i}} \tag{5}$$

defined as the ratio of the constraint gradient matrix N_{ij} being the derivative of the jth constraint z_j with respect to the ith variable x_i, and of the objective function gradient vector ∇F_i. The OC algorithm applied here includes two intertwined loops

- *scaling*: moves constraints to the feasible space in such a way that at least one constraint is active,
- *resizing*: concludes the previous cycle and initiates a new scaling procedure by making a jump in the search space to significantly reduce the objective function value, and
- these two loops are dependent on m active constraints that need to be determined.

The overall progress of scaling versus resizing is in the direction of objective function reduction, otherwise a stopping condition should halt the optimization process [8,19,21]. The OC pseudocode is presented here (Table 1) in brief.

The following Secs. 5.1–5.6 discuss how to formulate the objective function and calculate the ratio of the sensitivity derivatives (5) in the context of multimaterial optimization of discrete lattice structure designs considering displacement constraints. Also, in brief, the algorithm details including the resizing and scaling steps together with the optimization stopping condition are described.

5.1 Optimization Problem and Objective Function Definition. With respect to structural optimization and lightweight design, the overall objective is formulated as a mass minimization problem and stated as

$$\text{minimize } F(\mathbf{x}) = \sum_{i=1}^{n} Al_i\rho_i(x_i) \tag{6}$$

where A is the cross-sectional area of a solid, round truss member, l_i is the length of each of the truss members, and ρ_i is the material density of each member as a function of Young's moduli x_i. This is subject to a set of m inequality displacement constraints δ_j

$$\delta_j(\mathbf{x}) \le \bar{\delta}_j \quad j = 1, 2, \ldots, m \tag{7}$$

The design variable vector $\mathbf{x}$ is bounded from both sides with $\bar{\bar{x}}_i$ and $\bar{x}_i$ as the upper and the lower boundaries

$$\bar{\mathbf{x}} \le \mathbf{x} \le \bar{\bar{\mathbf{x}}} \tag{8}$$

The dependency expressed in $\rho_i = \rho_i(x_i)$ is obtained through material testing, as provided in Eq. (3). This dependency effectively enables the optimization procedure to use Young's modulus, x_i, as a design variable while keeping the cross-sectional area as a fixed parameter within the optimization.

The expressions that follow are derived considering a continuous variable and linear elastic model of the discrete lattice structure behavior. Given Eqs. (2) and (3) to express the dependency $\rho_i = \rho_i(x_i)$ in terms of the design variables provides the following formulation of the objective function $F(\mathbf{x})$:

$$F(\mathbf{x}) = \sum_{i=1}^{n} Al_i \left[c - \frac{\log\left(\dfrac{\bar{\bar{x}}_i - \bar{x}_i}{x_i - \bar{x}_i} - 1\right)}{p} \right] \tag{9}$$

as well as of its gradient ∇F_i

$$\nabla F_i = \frac{\partial F}{\partial x_i} = Al_i \frac{\partial \rho_i}{\partial x_i} = -\frac{Al_i(\bar{x}_i - \bar{\bar{x}}_i)}{p\ln(10)(\bar{x}_i - x_i)^2\left(\dfrac{\bar{x}_i - \bar{\bar{x}}_i}{\bar{x}_i - x_i} - 1\right)} \tag{10}$$

with $c = 1.16$ and $p = 57.46$ as the curve fitting coefficients obtained from the material properties testing (please refer to Sec. 4.2 for details on how the coefficients are obtained).

5.2 Constraints Definition. To optimize lattice structure designs, this work considers the application of displacement constraints for which a virtual load is applied to obtain the displacement gradients by imposing a unit load in the direction specified by the individual constraint. Thus, by considering the linear elastic model of the lattice structure and the respective solution of the equilibrium equation

$$\mathbf{f} = \mathbf{K}\mathbf{u} \tag{11}$$

where $\mathbf{f}$ is the load vector, $\mathbf{K}$ is the global stiffness matrix, and $\mathbf{u}$ is the nodal displacement vector, then the displacement constraints calculation can be incorporated in the solution of Eq. (11) with the least amount of additional computational expenses by addition of virtual load vectors for each of the jth constraints

Table 1 The OC algorithm pseudocode

```
1: ν ← 0 ;
2: x ← Initialize variable vector of size i;
3: while ∼(Stopping conditions) do
4:     F(x), ∇F_i ← Objective function evaluation and gradients calculation;
5:     z_j(x) ← Compute and classify constraints, decision on scaling or resizing;
6:     N_ij ← Compute constraint gradients;
7:     λ_j ← Based on e_ij compute Lagrangian multipliers so that m constraints are independent;
8:     if "scaling" then
9:         x ← Scaling to constraint boundary surface;
10:    else
11:        x ← Resizing based on λ_j and e_ij;
12:    fi
13:    ν ← ν + 1;
14: od
```

either as a single value or a linear combination of multiple displacements. Thus to express the constraints with respect to the virtual energy of the system a flexibility coefficient U_{ij} associated with the ith member and jth constraint is defined [8] as

$$U_{ij} = x_i \mathbf{u}_i^{\mathrm{T}} \mathbf{k}_i \mathbf{s}_i^j \tag{12}$$

where $\mathbf{u}_i^{\mathrm{T}}$ is a displacement vector, $\mathbf{k}_i$ is the local truss element stiffness matrix, and $\mathbf{s}_i^j$ is the displacement vector corresponding to the imposed virtual load vector. As both A and E participate linearly in the stiffness of truss members, then the displacement constraint δ_j with respect to the flexibility of the system U_{ij}, constraint boundary $\bar{\delta}_j$, and Young's modulus x_i is expressed as

$$\delta_j = \frac{U_{ij}}{x_i} \leq \bar{\delta}_j \tag{13}$$

Providing Eq. (13), the gradient matrix N_{ij} of the jth displacement constraint δ_j with respect to the ith variable x_i and the flexibility U_{ij} is given as

$$N_{ij} = \frac{\partial \delta_j}{\partial x_i} = -\frac{U_{ij}}{x_i^2} \tag{14}$$

5.3 Constraint Activity and Lagrangian Multipliers. The solution of Eq. (4) requires both an independent set of active m constraints and that Eq. (4) is always solvable even if e_{ij} in Eq. (5) is not necessarily full rank. To assure the solution of Eq. (4), first a critical constraint is determined in the relation to the target response ratio β_j of each jth constraint δ_j with respect to its boundary $\bar{\delta}_j$

$$\beta_j = \frac{\bar{\delta}_j}{\delta_j} \tag{15}$$

Active constraints are then selected with reference to a critical constraint whose value, according to Eq. (15), is either in a feasible region close to or at its boundary, or in an infeasible region violating its boundary by the most with respect to the other constraints. In this context, Eq. (15) is a mean to assert the independent constraint set $\boldsymbol{C}$ resulting in either one of the following sets [8,19,21]:

$$\boldsymbol{C} = \begin{cases} 1.\ \text{The constraint nearest to its boundary and all contraints within a 3\% margin} \\ 2.\ \text{The most violated constraint and those within a 3\% margin to it} \\ 3.\ \text{Constraints which are at their boundaries within a 3\% margin} \end{cases} \tag{16}$$

Cases 1 and 3 in Eq. (16) require that all of the constraint values are in the feasible region, whereas case 2 allows for values both in feasible and infeasible regions. Second, according to Ref. [21], Eq. (4) is expanded by multiplication from both sides with the product of the ratio of the sensitivity derivatives e_{ij} calculated according to Eq. (5) and the diagonal weighting matrix $A_{ii} = \nabla F_i x_i$ that is obtained by multiplication of the ith objective function gradient (10) and the ith variable x_i. The overall expanded system of equations written in vector notation is given as follows [21]:

$$\begin{aligned} &\mathbf{H}\lambda = \mathbf{W} \\ &\text{where} \\ &\mathbf{H} = \mathbf{e}^{\mathrm{T}}\mathbf{A}\mathbf{e} \\ &\mathbf{W} = \mathbf{e}^{\mathrm{T}}\mathbf{A}1 \end{aligned} \tag{17}$$

According to Ref. [21], Eq. (17) will yield a set of Lagrangian multipliers indicating an independent set of constraints if all multipliers are negative. The necessary condition is that $\mathbf{H}$ is nonsingular and that the weighting matrix $\mathbf{A}$ is positive definite. If Eq. (17) yields both positive and negative Lagrangian multipliers, then the positive multipliers indicate constraint dependency requiring their deletion from the active constraint set and recalculation of Eq. (17) repeating the procedure until all multipliers are negative.

5.4 Resizing. After the Lagrangian multipliers are obtained by solving Eq. (17), the algorithm either resizes if the independent constraint set $\boldsymbol{C}$ is based on case 3 in Eq. (16), or applies a compound scaling [21] until the condition 3 in Eq. (16) is obtained thus completing an optimization cycle. The resizing formula derived from the optimality condition (4) is given with respect to cycle ν and a cycle step size factor α as

$$x_i^{\nu+1} = x_i^{\nu} \left[\sum_{j=1}^{m} e_{ij} \lambda_j \right]^{1/\alpha} \tag{18}$$

Equation (18) takes only positive sums into consideration. If there are no positive members then the corresponding variable is set to its lowest possible value as defined by the boundary $\bar{x}_i$. The initial value for step size factor α is taken as $\alpha = 2$; however in later steps, an interpolation scheme is implemented according to Refs. [8,19,21].

5.5 Scaling. In general, scaling identifies the most critical constraint and calculates the scaling factor Λ to move the constraint to its boundary [8]

$$x_i' = \Lambda x_i \tag{19}$$

The assumption is that all of the other constraints are also moved to the feasible space. However, this is not guaranteed for a nonlinear constraint set. Compound scaling as defined in Ref. [21] on the other hand is more robust as it scales the variables by analyzing the first-order Taylor approximation in the constraint response due to change in the variable vector. Each of the variables are classified as active or passive contributors to the constraint response change that enables the calculation of scaling factor vector Λ. For details on compound scaling, please refer to Ref. [42].

5.6 Optimization Stopping Conditions. The Kuhn–Tucker conditions provide only the necessary conditions for a local optimum and therefore do not assure that the global optimum is found. In this context, to prevent long executions times but still to assure good solutions, the stopping conditions are most often empirically defined [21]. For this work, the following stopping conditions $\boldsymbol{S}$ are specified:

$$S = \begin{cases} 1.\ \text{The iterration exceeds 500 steps} \\ 2.\ \text{The iterration exceeds 100 cycles} \\ 3.\ \text{Objective value ratio of two consecutive cycles} > 1.005 \\ 4.\ \text{Change in objective function in two consecutive cycles} < |0.002| \end{cases} \tag{20}$$

6 Results

This section presents results for two optimization studies that are relevant in the context of multimaterial AM and form the basis for investigating optimized multimaterial lattice design for customized products, e.g., a sports helmet. Both of the examples include a lattice structure that is characteristic of the optimizing material used to achieve a lightweight design under displacement constraints. For both optimization problems, a $10 \times 10 \times 10$ mm^3 cubic cell (Fig. 4) is used as the lattice building block with all solid, round cross-sectional member diameters fixed to 1 mm.

The generalized OC method for multimaterial optimization of discrete lattice structure designs is implemented in MATLAB together with a linear elastic finite element method (FEM) module module for design response analysis. Both of the optimization examples are run on a standard desktop machine with a central processing unit (CPU) with four cores, 8 MB cache, a clock speed of 3.30 GHz, and 8 GB of RAM with no parallel programming implementation.

6.1 Cubic Lattice Optimization Example. The first illustrative example is the optimization of a cubic lattice that is built from a $4 \times 4 \times 4$ matrix of unit cells, according to Fig. 4, resulting in the lattice shown in Fig. 5 with 64 cells and 604 truss members in total. The purpose of this example is to show that the optimization for mass given displacement constraints produces a solution that is lighter, and therefore higher performing, than a structure configured with a single material.

Boundary conditions for this example are specified according to Figs. 5 and 6, and a load of $F = 50.0$ N is applied in the negative z-direction and distributed among all of the top-face nodes. Truss elements that do not contribute to the overall response because they have two fixed nodes are removed from the structure, reducing the overall number of elements to 548. The displacement

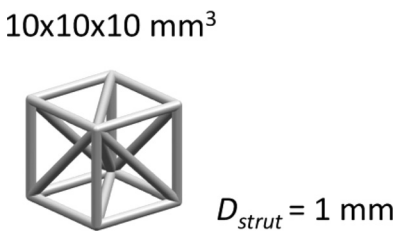

Fig. 4 Cubic cell definition

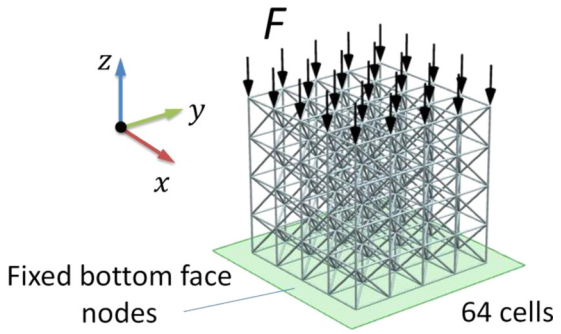

Fig. 5 Cube lattice topology and boundary conditions

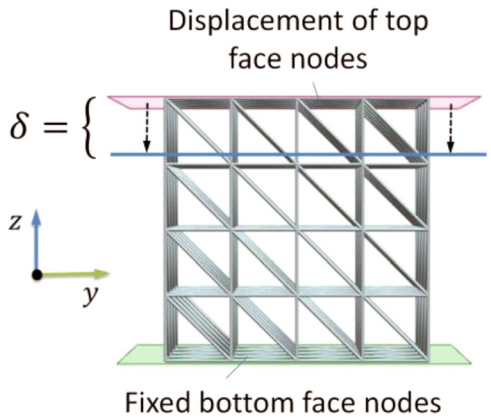

Fig. 6 Displacement constraint definition for cubic lattice

constraint of $\delta \leq 1$ mm per node is defined for each of the top-face nodes as shown in Fig. 6, resulting in a cumulative constraint of $\delta \leq 25$ mm. The bottom face nodes are fully fixed in x–y–z. All of the displacement constraints are calculated in the direction of the applied load.

For the optimization, two starting points are selected, one in the upper region of the Young's modulus variable span as $x_{1_i} = 3000$ MPa and the other as $x_{1_i} = 10$ MPa. Finally, the optimization problem with respect to Eq. (6) is formulated as

$$\begin{aligned} &\text{minimize } F(\mathbf{x}) = \sum_{i=1}^{n} AL_i \rho_i(x_i) \\ &\text{Subject to :} \\ &\quad \delta(\mathbf{x}) \leq 25.0\,\text{mm} \\ &\quad 8.3 \leq x_i \leq 3250\,\text{MPa} \end{aligned} \tag{21}$$

6.2 Cubic Lattice Optimization Results. The results of the optimization as specified by the optimization model in Eq. (21) are summarized as follows:

(a) For both starting points $x_{1_i} = 3000$ MPa and $x_{1_i} = 10$ MPa, the minimum mass obtained is $F(\mathbf{x}) = 5.87$ g and has a material distribution that is illustrated in Fig. 7.
(b) According to the stopping conditions (20), Fig. 8 shows the convergence of the optimization procedure at step 12 after completing four cycles for both starting points. The resizing points are denoted with $\times$ symbol, whereas the scaling procedure is denoted using the o symbol.
(c) The values of the cumulative displacement constraints are $\delta_1(\mathbf{x}) = 25$ mm and are evenly distributed among the 25 top-face points, almost equating to 1 mm per point. The highest deviation from any of the constraint points of the 1 mm boundary equates to 0.02 mm, which is acceptable.
(d) Given the material range of $8.3 \leq E \leq 3250$ MPa and a lattice topology according to Fig. 5, the same displacement is obtained when taking a single material of Young's modulus $E = 97$ MPa with a total mass of $m = 6.11$ g. A comparison to the obtained result of $F(\mathbf{x}) = 5.87$ g shows an improvement of 5% when optimizing over material properties while keeping the cross-sectional diameter fixed to 1 mm.
(e) The running time of the cubic lattice optimization is ~25 s.

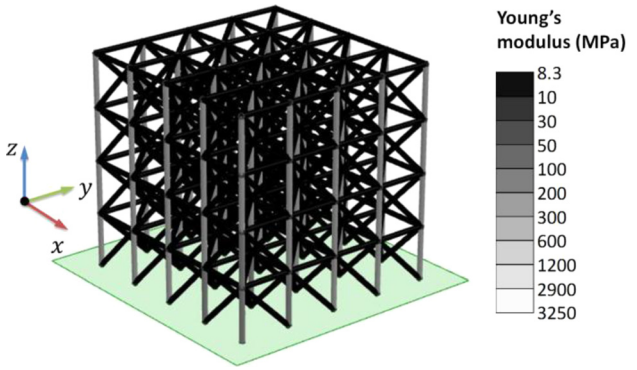

Fig. 7 Material distribution for cubic lattice optimization example

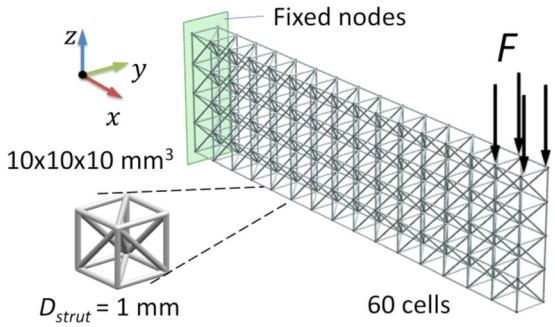

Fig. 9 Cantilever beam topology

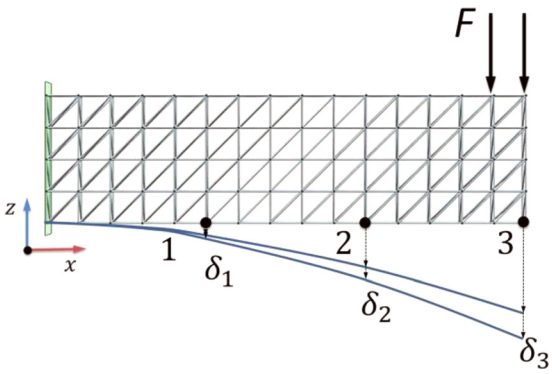

Fig. 10 Cantilever beam boundary conditions and constraints

6.3 Cantilever Beam Optimization Example. This example uses a cantilever beam optimization problem (Fig. 9) composed of a 15×4 matrix of cubic cells that are defined according to Fig. 4. The number of truss members is 677 in total.

The aim is to achieve the desired compliance and, if possible, to reduce the weight of the structure given the boundary conditions, loads, and displacement constraints that are defined for pairs of nodes that are equidistant from the support of the cantilever and where each pair is 50 mm apart measured over the bottom length of the cantilever beam. Truss elements that do not contribute to the overall response because they are fixed at both nodes are removed from the lattice reducing the overall number of elements, and design variables, to 660. Thus, this study serves to show that with multimaterial design optimization it is possible to achieve the prescribed displacement, which is constrained from both sides as $\bar{\delta} \leq \delta(\mathbf{x}) \leq \bar{\delta}$, while keeping the cross section of the truss members fixed.

The boundary conditions for this example are specified according to Fig. 10. The load of $F = 10.0$ N is distributed among the four nodes, two in-plane, on the top face of the cantilever beam, and the displacement constraints $0.8 \leq \delta_1 \leq 1.6$ mm, $12.0 \leq \delta_2 \leq 16.0$ mm, and $24.0 \leq \delta_3 \leq 30.0$ mm are prescribed for each of the nodal pairs identified. The far left face nodes are fully constrained in x–y–z. Our tests for using a single material taking $E = 3000$ MPa per strut yielded $\delta_1 = 0.76$ mm, $\delta_2 = 2.52$ mm, and $\delta_3 = 4.72$ mm based on the defined boundary conditions. Those results help specify the values, i.e., ranges, for the displacement constraint δ_1 of the stiff material in the multimaterial optimization model, while allowing significant displacement ranges for the constraints of other nodes, e.g., the soft material.

For the optimization, two starting points are selected: one in the upper region of the Young's modulus variable as $x_{1_i} = 3000$ MPa and the other as $x_{1_i} = 10$ MPa. Finally, the cantilever beam optimization problem is formulated as follows:

$$\begin{aligned} &\text{minimize } F(\mathbf{x}) = \sum_{i=1}^{n} AL_i \rho_i(x_i) \\ &\text{Subject to :} \\ &\quad 0.8 \leq \delta_1(\mathbf{x}) \leq 1.6\,\text{mm} \\ &\quad 12.0 \leq \delta_2(\mathbf{x}) \leq 16.0\,\text{mm} \\ &\quad 24.0 \leq \delta_3(\mathbf{x}) \leq 30.0\,\text{mm} \\ &\quad 8.3 \leq x_i \leq 3250\,\text{MPa} \end{aligned} \tag{22}$$

6.4 Cantilever Beam Optimization Results. The results of the optimization as specified by the optimization model in Eq. (22) are summarized as follows:

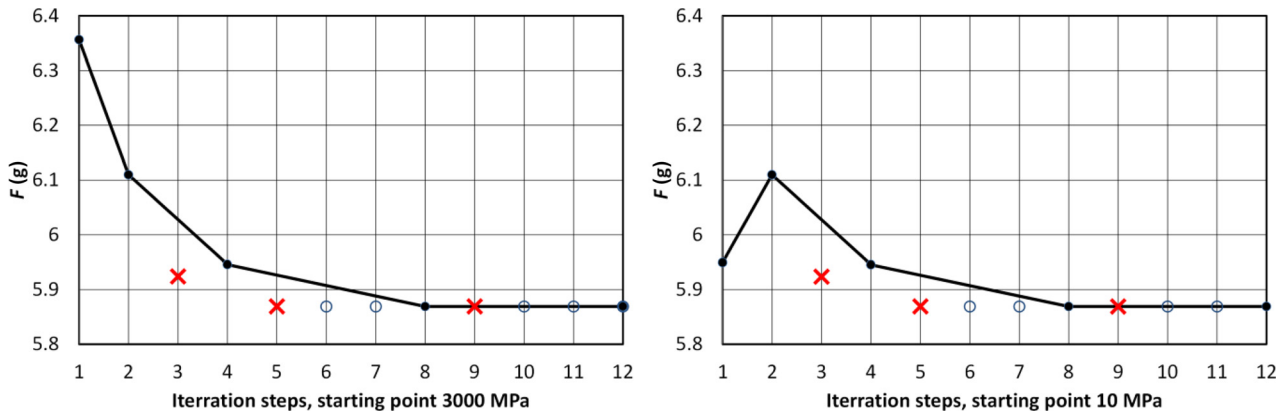

Fig. 8 The mass over iteration steps history for cubic lattice optimization: $x_{1_i} = 3000$ MPa starting point (left) and $x_{1_i} = 10$ MPa starting point (right)

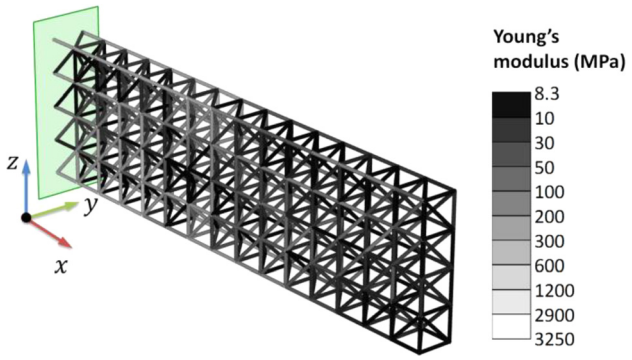

Fig. 11 Material distribution for the cantilever beam optimization with starting point $x_{1_i} = 3000$ MPa

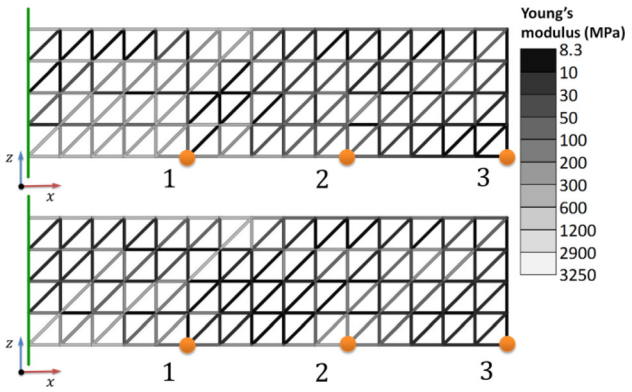

Fig. 12 Front views of material distribution for cantilever beam optimization: $x_{1_i} = 3000$ MPa starting point (top) and $x_{1_i} = 10$ MPa starting point (bottom)

(a) The minimum mass for the starting point $x_{1_i} = 3000$ MPa is $F(\mathbf{x}) = 7.12$ g resulting in the material distribution as shown in Figs. 11 and 12. The minimum mass for the starting point $x_{1_i} = 10$ MPa is $F(\mathbf{x}) = 7.06$ g.
(b) As shown in the iteration plots in Fig. 13, the optimization stops at the 500th step according to the stopping conditions in Eq. (20).
(c) The values of the displacement constraints for the first starting point are $\delta_1(\mathbf{x}) = 1.6$ mm, $\delta_2(\mathbf{x}) = 12$ mm, and $\delta_3(\mathbf{x}) = 30$ mm thus satisfying the constraints as shown in Fig. 13. For the second starting point, $x_{1_i} = 10$ MPa, the first displacement constraint equals $\delta_1(\mathbf{x}) = 1.46$ mm thus also being satisfied, but not located at the boundary. The other two constraints δ_2 and δ_3 are equal to the results with the starting point $x_{1_i} = 3000$ MPa. Figure 14 shows the x–z plane deformation results for the $x_{1_i} = 3000$ MPa starting point example. The allowed displacement span is shown with two parallel lines that define the possible range of values for each of the constrained node pairs.
(d) The running time of the cubic lattice optimization is ~48 min.

7 Discussion

A generalized OC method for optimization of AM multimaterial lattice structures is presented and tested on two examples. Discussion points focus on the specific phases of the DfAM multimaterial product design approach as implemented in this paper for material characterization and computational optimization, followed by their implications for developing and informing a complete product design methodology.

7.1 Empirical Studies for DfAM. New developments in AM technologies, particularly in inkjet 3D-printing, allow for on-the-fly mixture of multiple base materials in order to create submaterials resulting in a continuous transition between material properties. If three or more materials are used, it is possible to consider new material properties across a two or more dimensional material-property surface that covers large areas in strength versus density. On commercial printers, such as the one used in this work, restrictions are often made by the manufacturer such as limiting material mixing ratios that can impede a user from freely creating material combinations. For the printer investigated in this work, the provided material mixing ratios are based on color shades [39]. Since color shades do not correlate linearly with mechanical properties, an equal spacing between the color shades does not result in an equal spacing between material properties such as density. However, the different mixing ratios at a limited range of densities are still informative for predicting the theoretical values and curve for the Young's modulus values, as conducted in this work. These continuous curves would be generated based on a discrete set of data even if manufacturer constraints were lifted, and ideally should cover enough variable measurements to enable the identification of a mathematical function describing the data, such as the one developed for the Young's modulus and density in Fig. 3.

The unequal spacing in material densities based on software holds are likely a product of the visual effects that emerge such that adding a small amount of black material to a white base material has a large visual effect, whereas adding the same amount of white material to a black base material has a negligible effect.

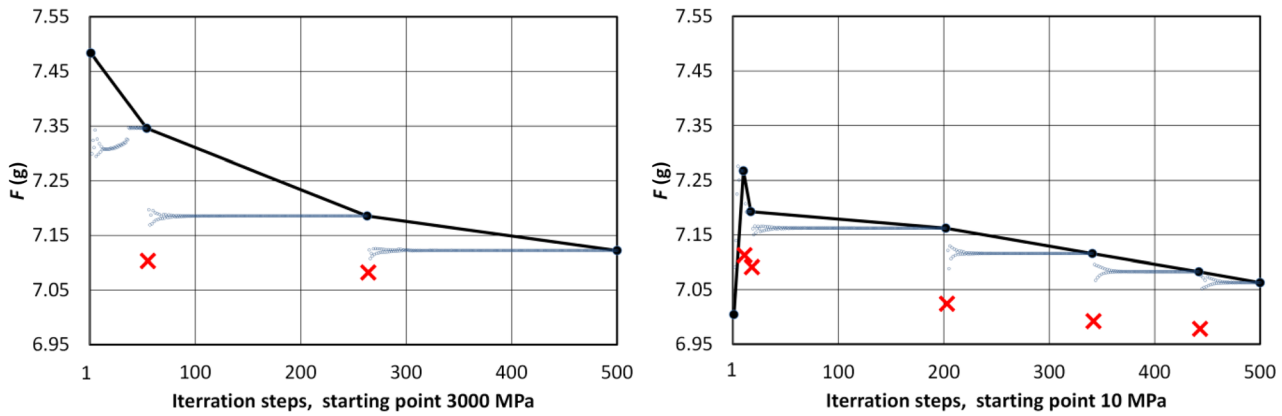

Fig. 13 Mass versus iteration step history: $x_{1_i} = 3000$ MPa starting point (left) and $x_{1_i} = 10$ MPa starting point (right)

These considerations are possible explanations for why the values of the high density white base material are closer together in terms of density than the ones with a black base material and why there are few density measurements available at densities that are representative of near equal mixes of materials. For the actual measurements collected, the higher values found for Young's modulus are considerably higher than manufacturer provided values, which possibly relates to a large number of in- and out-of-process parameters available for the inkjet 3D-printing process [40]. No information, besides the use of the ASTM D638-10 standard, is available on the testing procedure of the manufacturer; hence the properties are not directly comparable.

Generally mechanical properties scale with the density, e.g., low-density materials tend to have lower elastic moduli than materials with higher densities [43]. While the results presented are valid with respect to the AM machine tested, future work includes theoretical testing of the method for a problem with a more evenly spread distribution of Young's modulus versus density and identifying other AM processes that offer such a capability.

7.2 OC Method Application. The OC method extended to multimaterial optimization of a lattice structure under displacement constraints achieved a mass reduction while satisfying all of the imposed constraints for both studies. The optimization problem examples are developed because no other established benchmark examples for discrete lattice multimaterial optimization were found. The overall optimization results can be considered as acceptable as the overall material density range is itself narrow spanning from approximately 1.10–1.18 g/cm^3, as shown from the material testing in Fig. 3. The effect of this narrow material span is clearly visible in the results in Figs. 8 and 13 when considering two different initial starting points. The cubic lattice optimization example shows fast convergence for both examples and the distribution of material exactly as expected. The overall running time of ~24 s is extremely fast considering the number of 548 variables and the benchmark performance of other methods as shown in Fig. 2.

The resulting structure for the cantilever lattice example as shown in Figs. 11, 12, and 14 conforms well to the imposed boundary conditions. The distribution of stiff material in the first beam section before point 1 shown in Fig. 12 relates to the constraint δ_1 as it allows a very narrow range for both the $x_{1_i} = 3000$ MPa and $x_{1_i} = 10$ MPa starting point examples. For the midsection of the beam between points 1 and 2, as shown in Fig. 12, the distribution of the material favors more compliant material distribution at the bottom while retaining more stiff material at the top. This effect is more visible in the lighter solution resulting from the starting point, $x_{1_i} = 10$ MPa. However, as there were no other constraints implemented, a significant 6–8 mm displacement occurs in the z-direction, measured at the tip of the beam. This implies an addition of more constraints if this lateral displacement is to be reduced.

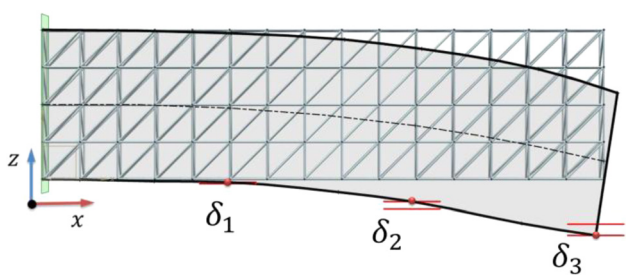

Fig. 14 Cantilever beam in plane displacement results for the $x_{1_i} = 3000$ MPa starting point. The allowed displacement range is shown with two parallel lines per each constrained node pair.

The algorithm had difficulties satisfying the narrow range of allowed displacements that are imposed by the constraints. This is visible in Fig. 13, which shows long scaling procedures per resizing cycle. Rather than converging on an optimum to halt the optimization either by relative or absolute changes in the objective function margins (19), the stopping criterion applied is a cut-off, which limits the duration of optimization runs. However, constraints that allow ranges, e.g., two inequality constraints, are not often applied with the OC method and how to handle this successfully is a potential future research direction. Considering the constraints that are imposed, both solutions are almost front and back face symmetric with respect to the material distribution. The other symmetries are difficult to assess especially in view of one cell thickness of the beam. The overall running time of ~48 min for the beam example is significantly higher than the cubic lattice optimization with a running time of ~24 s. It can be calculated that 12 iteration steps for the cantilever beam example have a running time of ~69 s, which is roughly 2.9 times longer than that of the cubic lattice example. As both examples have about the same number of truss members, but the cantilever has more constraints, it is concluded that it is the number of constraints that increases the optimization running time. This can be mitigated either by a parallel programming implementation, effectively reducing the number of iterations but not affecting the convergence process. To tackle the latter, the addition of other constraints and constraint types might support the convergence process if, an appropriate constraint handling strategy is applied with respect to the addition and removal of the constraints from the active constraint set.

The results presented in this study are achieved considering the following model simplifications, which will be addressed in future work:

(a) Young's modulus is considered as a continuous variable. While this is theoretically possible in inkjet 3D printing, the current machine only allows discrete material combinations. This exact case requires integer-based selection of materials, which might diminish the quality of the optimized design.
(b) Future extensions require the consideration of stress $\bar{\sigma} = \bar{\sigma}(E)$ and buckling $\bar{F}_B = \bar{F}_B(E)$ constraints, which are material dependent. Both of the constraints are considered as local constraints requiring more advanced constraint handling procedures, otherwise a heavy load on computational resources is imposed [33]. It is expected that the material dependency of both of the constraint boundaries presents far less of a problem then satisfying a large number of local constraints during scaling procedures.
(c) OC methods require knowledge of the constraint behavior with respect to their activity and optimum location to be successfully implemented. This will be investigated in the future to develop a generalized method for complex-shaped, multimaterial lattices fabricated with AM.

7.3 Implications for a DfAM Product Design Methodology. The empirical testing of materials, input of constraints into an optimization model, and optimization of a final structure are all developed in this paper as general methods within a DfAM product design methodology (Fig. 1). In this paper, the DfAM approach is implemented specifically for initial optimization examples characteristic of sports helmet design, such as maximizing performance through alteration of materials within a fixed volume. Particularly, the displacement constraints investigated in the paper form the basis of evaluation of structures for energy absorption, such that a structure should have some displacement to absorb energy, while not too much displacement that could harm a user. The additional example of a compliant beam that must meet a specific displacement over a series of points is representative of the need to design a structure that conforms to a user's head shape comfortably. The general approaches for empirical testing, constraint characterization, and computational optimization are demonstrated to support optimized design of multimaterial

lattice structures that outperform single material lattice structures. Once extended and generalized, the methods as a whole could form the basis for AM-based customized design for a variety of products beyond the helmet application. Future research will implement the final phase of the proposed DfAM process. This involves the testing of an optimized design to confirm the results and to potentially refine the models based on the compared performance of the optimization results with empirical measurements.

8 Conclusion

In this paper, an optimization approach using OC is developed to facilitate effective design of complex, multimaterial products for optimal performance within the confines of AM constraints. The optimization approach is developed in the context of designing multimaterial lattice structures as part of a larger DfAM methodology and product design cycle. An OC approach is utilized due to its potential effective use for optimizing large-scale discrete structures and the possibility to extend it for multimaterial applications. In order to adhere to DfAM considerations, empirical measurements are conducted to characterize the properties of two printable base materials. The materials consist of a low strength and high strength material that are combined through the AM process to form mixtures of materials with intermediate properties. These measured material properties are used to generate data curves that are utilized by the optimization algorithm for configuring multimaterial lattices for two problems that demonstrate a basis for the effective configuration of multimaterial products.

The application of the developed method resulted in the reduced mass of multimaterial lattices in both examples while satisfying the modeled constraints. More specifically, as shown in cubic lattice example, the results demonstrate that the use of multiple materials in lattice applications returned higher performance than similar structures using only a single material, thus motivating the need for multimaterial optimization approaches for product design. The developed method also exhibited difficulties in meeting the narrow range of displacement constraints in the second example resulting in slow convergence, which could possibly be mitigated both by including additional constraints, improving constraint handling and applying parallel programming techniques to improve the overall performance. The results and the study as a whole demonstrate the feasibility of the OC method in developing specific design optimization algorithms that adhere to DfAM constraints and enable the design of highly complex structures for multimaterial AM. The extension of the method beyond displacement constraints requires handling of dynamic stress and buckling stress constraints and the introduction of a discrete material selection procedure to adhere to current constraints of the AM machine. These considerations, in addition to empirical testing of fabricated, optimized structures are important for future development of these methods. Such advancements in optimization are crucial for leveraging the unique manufacturing capabilities of AM and developing new designs that surpass the performance of those limited by traditional manufacturing technologies.

Acknowledgment

Partial funding for this research is provided by ETH Zurich through the Seed Project, SP-MaP 02-14, "Additive Manufacturing of Complex-Shaped Parts With Locally Tunable Materials."

References

[1] Huang, S. H., Liu, P., Mokasdar, A., and Hou, L., 2013, "Additive Manufacturing and Its Societal Impact: A Literature Review," Int. J. Adv. Manuf. Technol., **67**(5–8), pp. 1191–1203.
[2] Vaezi, M., Chianrabutra, S., Mellor, B., and Yang, S., 2013, "Multiple Material Additive Manufacturing—Part 1: A Review: This Review Paper Covers a Decade of Research on Multiple Material Additive Manufacturing Technologies Which Can Produce Complex Geometry Parts With Different Materials," Virtual Phys. Prototyping, **8**(1), pp. 19–50.
[3] Beyer, C., 2014, "Strategic Implications of Current Trends in Additive Manufacturing," ASME J. Manuf. Sci. Eng., **136**(6), p. 064701.
[4] Hiller, J., and Lipson, H., 2009, "Design and Analysis of Digital Materials for Physical 3D Voxel Printing," Rapid Prototyping J., **15**(2), pp. 137–149.
[5] Gaynor, A. T., Meisel, N. A., Williams, C. B., and Guest, J. K., 2014, "Multiple-Material Topology Optimization of Compliant Mechanisms Created Via PolyJet Three-Dimensional Printing," ASME J. Manuf. Sci. Eng., **136**(6), p. 061015.
[6] Hammetter, C., Rinaldi, R., and Zok, F., 2013, "Pyramidal Lattice Structures for High Strength and Energy Absorption," ASME J. Appl. Mech., **80**(4), p. 041015.
[7] Bendsoe, M. P., and Sigmund, O., 2003, *Topology Optimization: Theory, Methods and Applications*, Springer-Verlag, Berlin, Germany.
[8] Khot, N., 1981, "Algorithms Based on Optimality Criteria to Design Minimum Weight Structures," Eng. Optim., **5**(2), pp. 73–90.
[9] Jamiolahmadi, S., and Barari, A., 2014, "Surface Topography of Additive Manufacturing Parts Using a Finite Difference Approach," ASME J. Manuf. Sci. Eng., **136**(6), p. 061009.
[10] Ma, R. R., Belter, J. T., and Dollar, A. M., 2015, "Hybrid Deposition Manufacturing: Design Strategies for Multi-Material Mechanisms Via 3D-Printing and Material Deposition," ASME J. Mech. Rob., **7**(2), p. 021002.
[11] Nelaturi, S., Kim, W., Rangarajan, A., and Kurtoglu, T., 2014, "Manufacturability Feedback and Model Correction for Additive Manufacturing," ASME Paper No. DETC2014-34222.
[12] Hu, Y., Fadel, G. M., Blouin, V. Y., and White, D. R., 2006, "Optimal Design for Additive Manufacturing of Heterogeneous Objects Using Ultrasonic Consolidation," Virtual Phys. Prototyping, **1**(1), pp. 53–62.
[13] Begley, M. R., and Zok, F. W., 2014, "Optimal Material Properties for Mitigating Brain Injury During Head Impact," ASME J. Appl. Mech., **81**(3), p. 031014.
[14] KrzeminskI, D. E., Goetz, J. T., Janisse, A. P., Lippa, N. M., Gould, T. E., Rawlins, J. W., and Piland, S. G., 2011, "Investigation of Linear Impact Energy Management and Product Claims of a Novel American Football Helmet Liner Component," Sports Technol., **4**(1–2), pp. 65–76.
[15] Hammetter, C., and Zok, F., 2014, "Compressive Response of Pyramidal Lattices Embedded in Foams," ASME J. Appl. Mech., **81**(1), p. 011006.
[16] Stanković, T., Mueller, J., Egan, P., and Shea, K., 2015, "Optimization of Additively Manufactured Multi-Material Lattice Structures Using Generalized Optimality Criteria," Computers and Information in Engineering Conference, Boston, ASME Paper No. DETC2015-47403.
[17] Hansen, K., Dau, N., Feist, F., Deck, C., Willinger, R., Madey, S. M., and Bottlang, M., 2013, "Angular Impact Mitigation System for Bicycle Helmets to Reduce Head Acceleration and Risk of Traumatic Brain Injury," Accid. Anal. Prev., **59**, pp. 109–117.
[18] Benson., B. W., Hamilton, G. M., Meeuwisse, W. H., McCrory, P., and Dvorak, J., 2009, "Is Protective Equipment Useful in Preventing Concussion? A Systematic Review of the Literature," Br. J. Sports Med., **43**(1), pp. i56–i67.
[19] Venkayya, V. B., 1978, "Structural Optimization: A Review and Some Recommendations," Int. J. Numer. Methods Eng., **13**(2), pp. 203–228.
[20] Venkayya, V. B., 1989, "Optimality Criteria: A Basis for Multidisciplinary Design Optimization," Comput. Mech., **5**(1), pp. 1–21.
[21] Venkayya, V. B., Tischler, V. A., Kolonay, R. M., and Canfield, R. A., 1990, "A Generalized Optimality Criteria Method for Mathematical Optimization," SIAM Conference on Geometric on Industrial Design Theory, Wright-Patterson Air Force Base, OH, pp. 124–153.
[22] Chang, P. S., and Rosen, D. W., 2013, "The Size Matching and Scaling Method: A Synthesis Method for the Design of Mesoscale Cellular Structures," Int. J. Comput. Integr. Manuf., **26**(10), pp. 907–927.
[23] Chu, J., Engelbrecht, S., Graf, G., and Rosen, D. W., 2010, "A Comparison of Synthesis Methods for Cellular Structures With Application to Additive Manufacturing," Rapid Prototyping J., **16**(4), pp. 275–283.
[24] Ning, X., and Pellegrino, S., 2012, "Design of Lightweight Structural Components for Direct Digital Manufacturing," 53rd AIAA/ASME/ASCE/AHS/ASC Structures, Structural Dynamics and Materials Conference, Honolulu, p. 1807.
[25] Shea, K., and Smith, I. F., 2006, "Improving Full-Scale Transmission Tower Design Through Topology and Shape Optimization," J. Struct. Eng., **132**(5), pp. 781–790.
[26] Doubrovski, Z., Verlinden, J. C., and Geraedts, J. M., 2011, "Optimal Design for Additive Manufacturing: Opportunities and Challenges," ASME 2011 International Design Engineering Technical Conferences and Computers and Information in Engineering, Washington, DC, August 28–31, ASME Paper No. DETC2011-48131.
[27] Eiamsa-ard, K., Ruan, J., Ren, L., and Liou, F. W., 2005, "Building Sequence of Boundary Model in Layered Manufacturing," ASME 2005 International Design Engineering Technical Conferences and Computers and Information in Engineering (DETC2005-85163), Long Beach, CA, September 24–28, ASME Paper No. (DETC2005-85163).
[28] Routhu, S., Kanakanala, D., Ruan, J., Liu, X. F., and Liou, F., 2010, "2-D Path Planning for Direct Laser Deposition Process," ASME 2010 International Design Engineering Technical Conferences and Computers and Information in Engineering Montreal, QC, Canada, January 01, 2010 ASME Paper No. CP00201004409000041500000l.
[29] Skouras, M., Thomaszewski, B., Coros, S., Bickel, B., and Gross, M., 2013, "Computational Design of Actuated Deformable Characters," ACM Trans. Graphics (TOG), **32**(4), pp. 1–9.
[30] Hiller, J., and Lipson, H., 2012, "Automatic Design and Manufacture of Soft Robots," IEEE Trans. Rob., **28**(2), pp. 457–466.
[31] Hu, Y., Blouin, V. Y., and Fadel, G. M., 2008, "Design for Manufacturing of 3D Heterogeneous Objects With Processing Time Consideration," ASME J. Mech. Des., **130**(3), p. 031701.

[32] Prager, W., 1968, "Optimality Criteria in Structural Design," Proc. Natl. Acad. Sci. U. S. A., **61**(3), pp. 794–796.
[33] Zhou, M., and Rozvany, G., 1992, "DCOC: An Optimality Criteria Method for Large Systems. Part I: Theory," Struct. Optim., **5**(1–2), pp. 12–25.
[34] Khot, N., Venkayya, V. B., and Berke, N., 1976, "Optimum Structural Design With Stability Constraints," Int. J. Numer. Methods Eng., **10**(5), pp. 1097–1114.
[35] Venkayya, V. B., and Khot, N., 1975, "Design of Optimum Structures to Impulse Type Loading," AIAA J., **13**(8), pp. 989–994.
[36] Flager, F., Soremekun, G., Adya, A., Shea, K., Haymaker, J., and Fischer, M., 2014, "Fully Constrained Design: A General and Scalable Method for Discrete Member Sizing Optimization of Steel Truss Structures," Comput. Struct., **140**, pp. 55–65.
[37] Grierson, D., and Chan, C.-M., 1993, "An Optimality Criteria Design Method for Tall Steel Buildings," Adv. Eng. Software, **16**(2), pp. 119–125.
[38] Venkayya, V., Khot, N., and Reddy, V., 1969, "Energy Distribution in an Optimum Structural Design," Air Force Flight Dynamics Lab, Wright-Patterson, OH, Report No. AFFDL-TR-68-156.
[39] Stratasys, Ltd., 2015, "Digital Materials (DMs) Data Sheet," http://www.stratasys.com/~/media/Main/Secure/Material%20Specs%20MS/PolyJet-Material-Specs/Digital_Materials_Datasheet.pdf
[40] Mueller, J., Kim, S., Shea, K., and Daraio, C., 2015, "Tensile Properties of PolyJet 3D-Printed Parts: Critical Process Parameters and How to Efficiently Analyze Them," ASME 2015 International Computers and Information in Engineering, Boston, MA, ASME Paper No. DETC2015-48024.
[41] Stratasys, Ltd., 2015, "Objet Connex 3D-Printers," http://www.stratasys.com/3d-printers/design-series/connex-systems and http://www.stratasys.com/~/media/en/Industries/Education/Resources/SSYS-EDU-LessonGuides-Glider-11-13.pdf
[42] Venkayya, V. B., and Tischler, V. A., 1989, *A Compound Scaling Algorithm for Mathematical Optimization*, Air Force Flight Dynamics Lab, Wright-Patterson, OH.
[43] Ashby, M. F., 1999, *Materials Selection and Process in Mechanical Design*, Butterworth Heinemann, Oxford, UK.